

# Radiative decay probabilities of the $(2s^2 2p_{1/2}^5 3s_{1/2})_{J=0}$ level in neonlike ions

P. Beiersdorfer,<sup>1,2</sup> M. Obst,<sup>2,3</sup> and U. I. Safronova<sup>4</sup>

<sup>1</sup>Lawrence Livermore National Laboratory, Livermore, California 94550, USA

<sup>2</sup>Space Sciences Laboratory, University of California, Berkeley, California 94720, USA

<sup>3</sup>Dr. Karl Remeis-Observatory & ECAP, University of Erlangen-Nuremberg, D-96049 Bamberg, Germany

<sup>4</sup>Physics Department, University of Nevada, Reno, Nevada 89557, USA

(Received 13 October 2010; published 24 January 2011)

The radiative decay rates of the  $(2s^2 2p_{1/2}^5 3s_{1/2})_{J=0}$  level in neonlike ions have been calculated for nuclear charges ranging from  $Z = 10$  to  $Z = 110$ . The calculations include the magnetic dipole decay to the  $(2s^2 2p_{3/2}^5 3s_{1/2})_{J=1}$  level, which is shown to be the dominant decay branch in low- $Z$  and very-high- $Z$  ions, as well as the two-electron, one-photon decays to the  $(2s^2 2p_{3/2}^5 3p_{1/2})_{J=1}$  and  $(2s^2 2p_{3/2}^5 3p_{3/2})_{J=1}$  levels, which dominate near  $Z = 50$ . We also take into account a small magnetic quadrupole decay branch to the  $(2s^2 2p_{3/2}^5 3s_{1/2})_{J=2}$  level and calculate the total radiative lifetime of the  $(2s^2 2p_{1/2}^5 3s_{1/2})_{J=0}$  level. The resulting values span over 15 orders of magnitude, and much of this range is accessible with modern atomic lifetime measurement techniques. In particular, we calculate a value of  $1.6 \times 10^4 \text{ s}^{-1}$  for the radiative decay rate of the  $(2s^2 2p_{1/2}^5 3s_{1/2})_{J=0}$  level in Fe XVII and show that the corresponding magnetic dipole transition has a measurable spectral intensity for electron densities below about  $1 \times 10^{13} \text{ cm}^{-3}$ .

DOI: [10.1103/PhysRevA.83.012514](https://doi.org/10.1103/PhysRevA.83.012514)

PACS number(s): 32.70.Cs, 32.30.Rj, 32.30.Jc, 32.70.Fw

## I. INTRODUCTION

Metastability, the fact that an excited level cannot decay by an electric dipole ( $E1$ ) allowed transition and thus may have a radiative lifetime many orders of magnitude larger than those levels that decay by electric dipole transitions, plays an important role in spectral line formation. The radiative rate has to compete with collisional processes, which may not only populate but also depopulate the excited level. As a result, radiative transitions from metastable levels are often a sensitive indicator of electron density and thus can be used for plasma diagnostics. Because of this sensitivity to plasma conditions, complete accounting of all radiative and collisional processes must be included in a kinetic model aimed at reproducing an observed spectrum.

The  $L$ -shell x-ray spectrum of neonlike ions contains several lines from metastable levels, which may be observed under the right conditions. For example, there are several electric quadrupole ( $E2$ ) transitions from upper levels  $2s^2 2p^5 3p$  and  $2s 2p^6 3d$  to the closed-shell  $(2s^2 2p^6)_{J=0}$  ground state that have been detected [1–4], and some of these transitions have been used for plasma diagnostics [5]. The lowest excited level in neonlike ions, the  $(2s^2 2p_{3/2}^5 3s_{1/2})_{J=2}$  level, decays by a magnetic quadrupole ( $M2$ ) transition to the ground state. The x-ray line produced by this decay was shown to be sensitive not only to electron density [6–8] but also to strong photon fields [9,10].

Among the  $2s^2 2p^5 3s$  levels, there is another metastable level, i.e., the  $(2s^2 2p_{1/2}^5 3s_{1/2})_{J=0}$  level. In neonlike ions with low atomic number  $Z$ , such as argon ( $Z = 18$ ) or iron ( $Z = 26$ ), this level is the third-lowest excited level. As we show below, relativistic effects rearrange energy levels depending on the angular momentum ( $j = 1/2$  or  $j = 3/2$ ) of the  $2p^5$  configuration, and this particular level moves higher in energy relative to its nearest neighbors as  $Z$  increases. In principle, this level cannot directly decay to the  $J = 0$  neonlike ground state, because  $J = 0 \rightarrow J = 0$  transitions are strictly forbidden. In low- $Z$  ions this level has two modes of radiative decay.

The first is via a magnetic dipole ( $M1$ ) transition to the  $(2s^2 2p_{3/2}^5 3s_{1/2})_{J=1}$  level, which is the second-lowest excited level in these neonlike ions. Because the energy splitting between these two levels is small, the associated spectral line is typically in the ultraviolet. For example, this line of Fe XVII has been observed at 1153 Å in the sun using the Solar Ultraviolet Measurements of Emitted Radiation (SUMER) instrument on the Solar and Heliospheric Observatory (SOHO) spacecraft [11]. As the level decays by the  $M1$  transition, it populates the  $(2s^2 2p_{3/2}^5 3s_{1/2})_{J=1}$  level, which in turn decays by a strong  $E1$  x-ray transition to ground. The second mode of decay is via a transition directly to the ground state, provided a strong enough ambient or nuclear magnetic field is present [12]. This Zeeman or hyperfine induced transition to the ground state results in an x-ray line, which has been observed, for example, in Ar IX at 47 Å in the electron beam ion trap at Livermore [12,13]. Both decay modes of the  $(2s^2 2p_{1/2}^5 3s_{1/2})_{J=0}$  level are very slow compared to typical rates of  $E1$  decay from other excited levels in the neonlike ion.

The aim of this paper is to tabulate the  $M1$  radiative decay rates of the  $(2s^2 2p_{1/2}^5 3s_{1/2})_{J=0}$  level as well as the corresponding transition energies, because this rate can now, in principle, be measured experimentally with modern ion trapping techniques [14]. Our work thus extends more general, previous calculations of neonlike ions [15–23] to a specific level that might be studied in the future. In fact, the decay of this level was noted in a recent measurement of the transition rate of the  $M2$  decay of the  $(2s^2 2p_{3/2}^5 3s_{1/2})_{J=2}$  level [24], although no experimental rate was assigned. A measurement of the  $M1$  decay rate would be a test of atomic theory in a range where very few data exist.

In the following we present calculations of the  $(2s^2 2p_{1/2}^5 3s_{1/2})_{J=0}$  level energies,  $M1$  decay rates, and transition energies as a function of atomic number calculated both with the flexible atomic code (FAC) [25] and with relativistic many-body perturbation theory (RMBPT) [26]. We also present calculations of the intensity of the  $M1$  transition relative to the prominent and well known  $n = 3 \rightarrow n = 2$

x-ray transitions in Fe XVII, which has been one of the most studied neonlike ions because its radiation is prominent in most laboratory and astrophysical high-temperature plasmas [27–32].

## II. THEORETICAL TECHNIQUES

The flexible atomic code is a fully relativistic atomic physics package based on the Dirac equation and described by Gu [25]. Radiative transition rates are calculated in the single multipole approximation. The fully relativistic approach of Grant [33] is used for calculating the  $M1$  transition rate; the nonrelativistic limit is used for electric dipole rates.

Although FAC was developed only rather recently, it has already been used extensively for the calculation of atomic data [34–36]. The recent measurement of the radiative decay rate of the  $(2s^2 2p_{3/2}^5 3s_{1/2})_{J=2}$  level [24] provided a first test of FAC calculations of radiative rates, and excellent agreement between the calculated value of  $2.06 \times 10^5 \text{ s}^{-1}$  and the measured value of  $(2.04^{+0.03}_{-0.09}) \times 10^5 \text{ s}^{-1}$  was found. That particular FAC calculation involved a 37-level model; that is, only the ground level and the 36 excited levels with a hole in the  $n = 2$  shell and a valence electron in the  $n = 3$  shell were included in the calculation. For the present paper, we use exactly the same 37-level calculation to determine the level energies and radiative transition rates.

FAC also allows the calculation of electron-impact excitation rates and the construction of a collisional-radiative model [34]. We used this feature to calculate the intensity of the spectral emission of Fe XVII and thus to predict the intensity of the  $(2s^2 2p_{1/2}^5 3s_{1/2})_{J=0} \rightarrow (2s^2 2p_{3/2}^5 3s_{1/2})_{J=1}$  transition that might be observed in future electron beam ion trap experiments. The FAC calculations furthermore provide a prediction of the sensitivity of the  $(2s^2 2p_{1/2}^5 3s_{1/2})_{J=0} \rightarrow (2s^2 2p_{3/2}^5 3s_{1/2})_{J=1}$  transition to the electron density.

We have also calculated the line strengths and transition rates for transitions between  $2s^2 2p^5 3s$ ,  $2s^2 2p^5 3d$ , and  $2s 2p^6 3p$  odd-parity levels in neonlike ions using the RMBPT. Details of this method for multipole transitions in hole-particle states were presented by Safronova *et al.* [26]. The calculations were carried out using sets of Dirac-Fock basis orbitals. The orbitals used in the present calculation were obtained as linear combinations of  $B$  splines. These  $B$ -spline basis orbitals were determined using the method described by Johnson *et al.* [37]. We used 50  $B$  splines of order 10 for each single-particle angular momentum state, and we included all orbitals with orbital angular momentum  $l \leq 9$  in our basis set.

## III. RESULTS

A Grotrian diagram of the lowest eight energy levels in neonlike iron, as calculated by FAC, is shown in Fig. 1. The diagram also shows the radiative decay paths. Among these levels, there are only two electric dipole-allowed transitions to the  $(2s^2 2p^6)_{J=0}$  ground state. The  $(2s^2 2p_{1/2}^5 3s_{1/2})_{J=0}$  level (level 3 in the figure) can only decay by a magnetic dipole transition to the  $(2s^2 2p_{3/2}^5 3s_{1/2})_{J=1}$  level. Electric quadrupole decay to the  $(2s^2 2p_{3/2}^5 3s_{1/2})_{J=2}$  level is, in principle, also possible. Our FAC calculations, however, show that this rate is

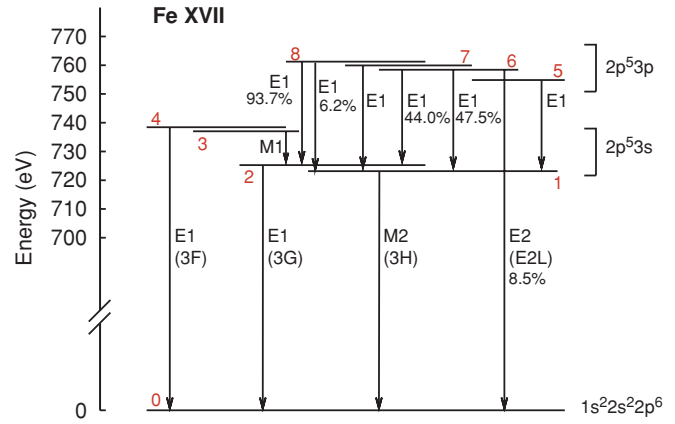


FIG. 1. (Color online) Grotrian diagram of the lowest eight excited levels in neonlike iron. Levels are labeled by their ordering in the FAC calculations. In particular, levels 1–8 are  $(2p_{3/2}^5 3s_{1/2})_{J=2}$ ,  $(2p_{3/2}^5 3s_{1/2})_{J=1}$ ,  $(2p_{1/2}^5 3s_{1/2})_{J=0}$ ,  $(2p_{1/2}^5 3s_{1/2})_{J=1}$ ,  $(2p_{3/2}^5 3p_{1/2})_{J=1}$ ,  $(2p_{3/2}^5 3p_{1/2})_{J=2}$ ,  $(2p_{3/2}^5 3p_{3/2})_{J=3}$ , and  $(2p_{3/2}^5 3p_{3/2})_{J=1}$ , respectively. Radiative decay paths are indicated by the multipole order of the decay. Only the strongest decay paths ( $>5\%$ ) are shown; hence, only one decay path is shown if it is used more than 95% of the time. The transitions to the ground state are labeled in the notation of [2].

about two orders of magnitude lower than the rate for magnetic dipole decay.

In the high- $Z$  limit, levels with a  $2p_{1/2}$  core vacancy group together, rising above levels with a  $2p_{3/2}$  core vacancy. In neonlike xenon, for example, the  $(2s^2 2p_{1/2}^5 3s_{1/2})_{J=0}$  level has energetically overtaken all  $2p_{3/2}$  core vacancy levels except one. The exception is the  $(2s^2 2p_{3/2}^5 3d_{5/2})_{J=1}$  level, which is

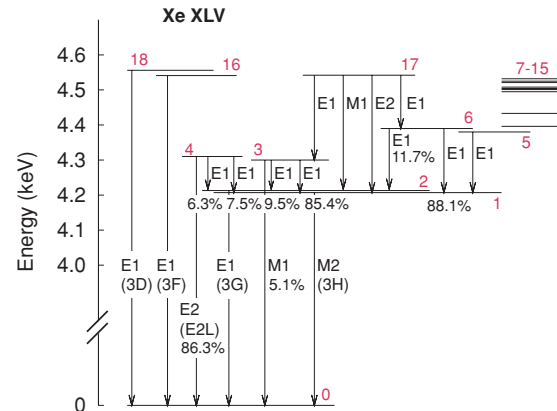


FIG. 2. (Color online) Grotrian diagram of the lowest 18 excited levels in neonlike xenon. Levels are labeled by their ordering in the FAC calculations. In particular, levels 1–6 are  $(2p_{3/2}^5 3s_{1/2})_{J=2}$ ,  $(2p_{3/2}^5 3s_{1/2})_{J=1}$ ,  $(2p_{1/2}^5 3s_{1/2})_{J=0}$ ,  $(2p_{1/2}^5 3s_{1/2})_{J=1}$ ,  $(2p_{3/2}^5 3p_{1/2})_{J=2}$ ,  $(2p_{3/2}^5 3p_{1/2})_{J=3}$ , and  $(2p_{3/2}^5 3p_{3/2})_{J=1}$ , respectively. Levels 16–18 are  $(2p_{1/2}^5 3s_{1/2})_{J=1}$ ,  $(2p_{1/2}^5 3s_{1/2})_{J=0}$ , and  $(2p_{3/2}^5 3d_{5/2})_{J=1}$ , respectively. Radiative decay paths are indicated by the multipole order of the decay. Only the strongest decay paths ( $>5\%$ ) are shown, and only one decay path is shown if it is used more than 95% of the time. The exception are the decay paths for level 17, which are to 00.1% to level 1, 27.2% to level 2, 70.6% to level 3, and 2.1% to level 6. The transitions to the ground state are labeled in the notation of [2].

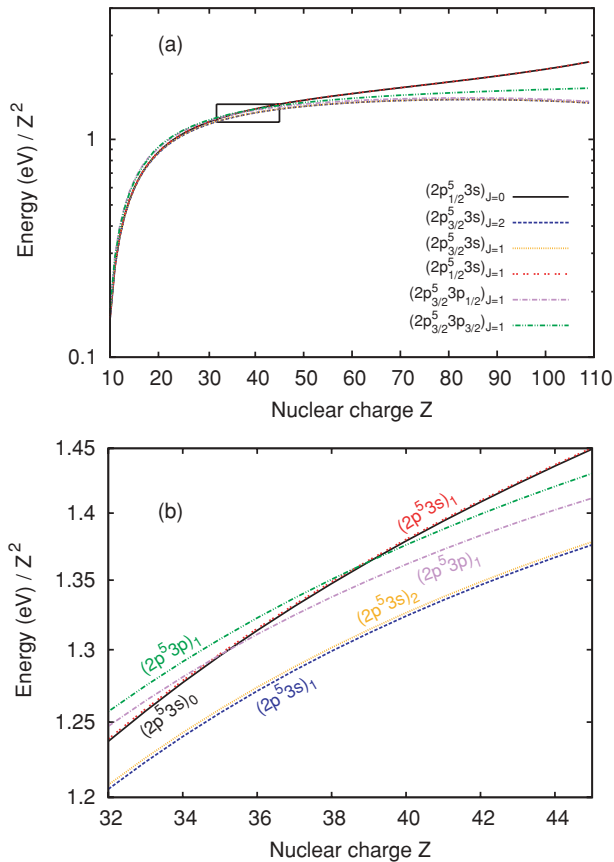


FIG. 3. (Color online) Dependence of the level structure of neonlike ions on the nuclear charge. The four levels with a  $3s$  valence electron are shown together with two levels having a  $3p$  valence electron. (a) The range between  $Z = 10$  and  $Z = 110$ ; (b) an expanded view showing the rearrangement of levels. The level energies are calculated with FAC.

level 18 in  $\text{Xe}^{44+}$ , as shown in the Grotrian diagram in Fig. 2. The decay of this level generally produces the brightest line in the neonlike x-ray spectrum for ions above krypton [38]. In addition, the  $(2s^2 2p_{1/2}^5 3s_{1/2})_{J=0}$  level has overtaken the  $(2s^2 2p_{3/2}^5 3p_{1/2})_{J=1}$  and  $(2s^2 2p_{3/2}^5 3p_{3/2})_{J=1}$  levels.

The rearrangement of the  $2p_{3/2}$  and  $2p_{3/2}$  levels is seen in Fig. 3. The  $(2s^2 2p_{1/2}^5 3s_{1/2})_{J=0,1}$  levels overtake the  $(2s^2 2p_{3/2}^5 3p_{1/2})_{J=1}$  and  $(2s^2 2p_{3/2}^5 3p_{3/2})_{J=1}$  levels between  $Z = 35$  and  $36$  and between  $Z = 39$  and  $40$ , respectively.

The  $(2s^2 2p_{1/2}^5 3s_{1/2})_{J=0,1}$  levels themselves stay close together, with a level separation of about 1–3 eV between  $Z = 20$  and  $Z = 110$ . This smoothly varying separation gets disrupted, however, near  $Z = 54$ . In this range of atomic numbers, the rearrangement of the  $2p_{1/2}$  and  $2p_{3/2}$  core vacancy levels leads to an avoided crossing of the  $(2s^2 2p_{1/2}^5 3s_{1/2})_{J=1}$  level and of the  $(2s^2 2p_{3/2}^5 3s_{1/2})_{J=1}$  level [2,39]. The disruptive effect of this avoided crossing is clearly seen in Fig. 4(b) by the discontinuity near  $Z = 54$ . The mutual “repulsion” of the  $(2s^2 2p_{1/2}^5 3s_{1/2})_{J=1}$  and  $(2s^2 2p_{3/2}^5 3s_{1/2})_{J=1}$  levels pushes the energy of the  $(2s^2 2p_{1/2}^5 3s_{1/2})_{J=1}$  level below that of the  $(2s^2 2p_{1/2}^5 3s_{1/2})_{J=0}$  level. In other words, for xenon and only for xenon, the energy of the  $(2s^2 2p_{1/2}^5 3s_{1/2})_{J=0}$  level is

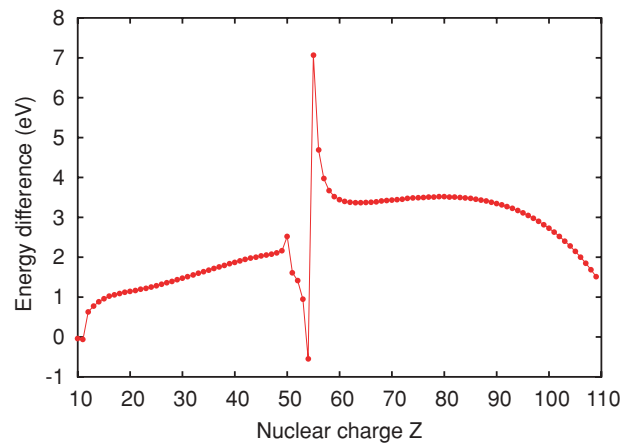


FIG. 4. (Color online) Separation of the  $(2s^2 2p_{1/2}^5 3s_{1/2})_{J=1}$  and  $(2s^2 2p_{1/2}^5 3s_{1/2})_{J=0}$  levels as a function of nuclear charge predicted by the FAC calculations. A negative value indicates that the energy of the  $(2s^2 2p_{1/2}^5 3s_{1/2})_{J=0}$  level is higher than that of the  $(2s^2 2p_{1/2}^5 3s_{1/2})_{J=1}$  level.

predicted to be higher than that of the  $(2s^2 2p_{1/2}^5 3s_{1/2})_{J=1}$  level. The difference is only 0.5 eV. Although our result agrees with that calculated by Ivanova and Gulov [20], experimental verification is needed, because the actual value of the  $(2s^2 2p_{1/2}^5 3s_{1/2})_{J=1}$  level energy is highly sensitive to configuration interaction at and near  $Z = 54$  and is thus somewhat uncertain.

The fact that the  $(2s^2 2p_{1/2}^5 3s_{1/2})_{J=0}$  level lies above the  $(2s^2 2p_{3/2}^5 3p_{1/2})_{J=1}$  level for  $Z \geq 36$  and above the  $(2s^2 2p_{3/2}^5 3p_{3/2})_{J=1}$  level for  $Z \geq 40$  means that two additional decay paths are open. Decay to either the  $(2s^2 2p_{3/2}^5 3p_{1/2})_{J=1}$  or the  $(2s^2 2p_{3/2}^5 3p_{3/2})_{J=1}$  level can proceed by an electric dipole transition. The rate is limited, however, by the fact that the vacancy must change angular momentum. The rate of the  $E1$  transition to the  $(2s^2 2p_{3/2}^5 3p_{1/2})_{J=1}$  level exceeds the  $M1$  decay rate until  $Z \approx 60$ . Above  $Z = 60$ , the  $M1$  decay dominates again. An overview of the rates calculated with FAC

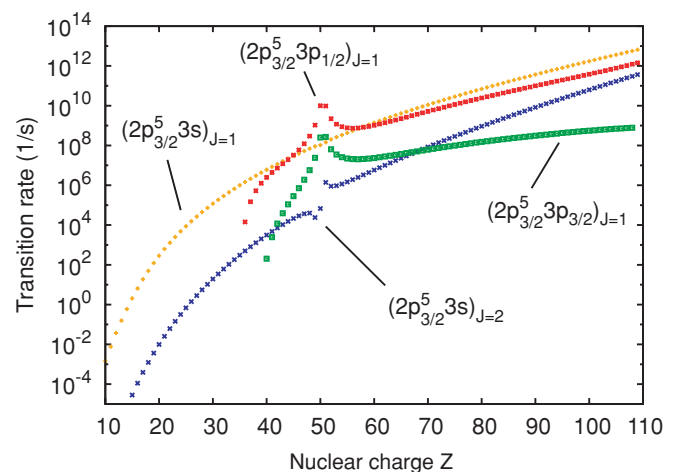


FIG. 5. (Color online) Radiative decay rates of the  $(2s^2 2p_{1/2}^5 3s_{1/2})_{J=0}$  level to various lower levels as a function of nuclear charge predicted by FAC calculations.

TABLE I. Wavelengths ( $\lambda$  in  $\text{\AA}$ ) and transition rates ( $A_r$  in  $\text{s}^{-1}$ ) for the  $(2s^2 2p_{1/2}^5 3s_{1/2})_{J=0} - (2s^2 2p_{3/2}^5 3s_{1/2})_{J=1}$   $M1$  transition in neonlike ions, evaluated in first-order (RMBPT-I) and second-order (RMBPT-II) relativistic many-body perturbation theory as well as with the relativistic atomic structure code FAC. The number in square brackets denotes the power of 10.

Z	RMBPT-I		RMBPT-II		FAC		Total Rate <sup>a</sup>
	$\lambda$	$A_r$	$\lambda$	$A_r$	$\lambda$	$A_r$	
13	54007.0	3.00[-1]	987167.0	4.91[-5]	68925.0	1.58[-1]	1.58[-1]
14	35933.0	9.94[-1]	81613.0	8.49[-2]	43874.0	5.97[-1]	5.97[-1]
15	24250.0	3.11[0]	36507.0	9.12[-1]	28736.0	2.05[0]	2.05[0]
16	16683.0	9.07[0]	17718.0	7.57[0]	19308.0	6.45[0]	6.45[0]
17	11721.0	2.46[1]	13162.0	1.74[1]	13288.0	1.86[1]	1.86[1]
18	8413.8	6.23[1]	9158.0	4.83[1]	9364.2	4.98[1]	4.98[1]
19	6170.1	1.48[2]	6523.8	1.25[2]	6754.2	1.23[2]	1.23[2]
20	4617.9	3.30[2]	4606.7	3.32[2]	4982.5	2.85[2]	2.85[2]
21	3522.3	6.98[2]	4168.4	4.21[2]	3753.9	6.20[2]	6.20[2]
22	2733.8	1.41[3]	2828.4	1.27[3]	2883.6	1.28[3]	1.28[3]
23	2155.3	2.74[3]	2203.2	2.56[3]	2254.2	2.53[3]	2.53[3]
24	1723.4	5.11[3]	1750.8	4.87[3]	1789.8	4.78[3]	4.78[3]
25	1395.6	9.25[3]	1412.3	8.92[3]	1441.0	8.74[3]	8.74[3]
26	1143.0	1.62[4]	1153.7	1.58[4]	1174.6	1.55[4]	1.55[4]
27	945.66	2.78[4]	952.73	2.72[4]	968.08	2.67[4]	2.67[4]
28	789.62	4.64[4]	794.42	4.56[4]	805.72	4.48[4]	4.48[4]
29	664.81	7.59[4]	668.14	7.48[4]	676.53	7.36[4]	7.36[4]
30	563.94	1.22[5]	566.30	1.20[5]	572.59	1.19[5]	1.19[5]
31	481.67	1.92[5]	483.36	1.90[5]	488.11	1.87[5]	1.87[5]
32	413.97	2.97[5]	415.21	2.94[5]	418.83	2.91[5]	2.91[5]
33	357.83	4.53[5]	358.80	4.49[5]	361.53	4.45[5]	4.45[5]
34	310.94	6.81[5]	311.68	6.76[5]	313.78	6.70[5]	6.70[5]
35	271.52	1.01[6]	272.08	1.00[6]	273.72	9.96[5]	9.96[5]
36	238.16	1.48[6]	238.59	1.47[6]	239.88	1.46[6]	1.48[6]
37	209.78	2.15[6]	210.12	2.13[6]	211.13	2.12[6]	2.27[6]
38	185.50	3.08[6]	185.77	3.06[6]	186.57	3.04[6]	3.57[6]
39	164.63	4.36[6]	164.84	4.34[6]	165.48	4.32[6]	5.59[6]
40	146.61	6.13[6]	146.78	6.11[6]	147.29	6.08[6]	8.58[6]
41	130.98	8.54[6]	131.11	8.51[6]	131.53	8.48[6]	1.29[7]
42	117.37	1.18[7]	117.47	1.18[7]	117.81	1.17[7]	1.91[7]
43	105.47	1.62[7]	105.55	1.61[7]	105.82	1.61[7]	2.80[7]
44	95.025	2.20[7]	95.096	2.19[7]	95.317	2.19[7]	4.15[7]
45	85.835	2.97[7]	85.893	2.96[7]	86.074	2.95[7]	6.28[7]
46	77.720	3.98[7]	77.768	3.96[7]	77.917	3.96[7]	1.00[8]
47	70.534	5.29[7]	70.573	5.27[7]	70.696	5.27[7]	1.76[8]
48	64.155	6.98[7]	64.187	6.96[7]	64.290	6.95[7]	3.73[8]
49	58.486	9.09[7]	58.509	9.07[7]	58.601	9.03[7]	1.17[9]
50	53.490	1.09[8]	53.486	1.09[8]	53.614	1.04[8]	1.03[10]
51	48.611	1.39[8]	48.684	1.38[8]	48.722	1.45[8]	1.00[10]
52	44.645	2.02[8]	44.675	2.01[8]	44.714	2.02[8]	2.47[9]
53	40.996	2.63[8]	41.018	2.62[8]	41.051	2.62[8]	1.48[9]
54	37.695	3.38[8]	37.713	3.37[8]	37.740	3.38[8]	1.24[9]
55	34.709	4.33[8]	34.724	4.31[8]	34.747	4.32[8]	1.22[9]
56	32.005	5.51[8]	32.018	5.49[8]	32.036	5.50[8]	1.31[9]
57	29.552	6.98[8]	29.565	6.96[8]	29.578	6.97[8]	1.48[9]
58	27.323	8.81[8]	27.333	8.78[8]	27.345	8.79[8]	1.73[9]
59	25.294	1.11[9]	25.304	1.10[9]	25.313	1.11[9]	2.04[9]
60	23.445	1.39[9]	23.453	1.38[9]	23.461	1.39[9]	2.45[9]
61	21.756	1.73[9]	21.764	1.73[9]	21.769	1.73[9]	2.95[9]
62	20.212	2.15[9]	20.219	2.15[9]	20.223	2.15[9]	3.57[9]
63	18.798	2.67[9]	18.804	2.66[9]	18.807	2.67[9]	4.33[9]
64	17.501	3.30[9]	17.507	3.29[9]	17.509	3.30[9]	5.25[9]
65	16.309	4.07[9]	16.315	4.06[9]	16.316	4.07[9]	6.37[9]
66	15.214	5.00[9]	15.219	4.99[9]	15.220	5.00[9]	7.71[9]
67	14.205	6.13[9]	14.210	6.11[9]	14.210	6.13[9]	9.34[9]

TABLE I. (Continued).

Z	RMBPT-I		RMBPT-II		FAC		Total Rate <sup>a</sup>
	$\lambda$	$A_r$	$\lambda$	$A_r$	$\lambda$	$A_r$	
68	13.275	7.49[9]	13.280	7.47[9]	13.279	7.49[9]	1.13[10]
69	12.416	9.13[9]	12.421	9.11[9]	12.420	9.13[9]	1.36[10]
70	11.623	1.11[10]	11.627	1.11[10]	11.626	1.11[10]	1.64[10]
71	10.889	1.35[10]	10.893	1.34[10]	10.892	1.35[10]	1.97[10]
72	10.209	1.63[10]	10.213	1.63[10]	10.211	1.63[10]	2.36[10]
73	9.579	1.97[10]	9.582	1.96[10]	9.581	1.97[10]	2.83[10]
74	8.994	2.37[10]	8.997	2.37[10]	8.995	2.37[10]	3.38[10]
75	8.450	2.85[10]	8.453	2.84[10]	8.452	2.85[10]	4.03[10]
76	7.945	3.42[10]	7.948	3.41[10]	7.946	3.42[10]	4.81[10]
77	7.474	4.10[10]	7.477	4.09[10]	7.475	4.10[10]	5.71[10]
78	7.036	4.90[10]	7.039	4.89[10]	7.037	4.90[10]	6.78[10]
79	6.627	5.85[10]	6.630	5.83[10]	6.628	5.85[10]	8.04[10]
80	6.245	6.97[10]	6.248	6.94[10]	6.246	6.96[10]	9.51[10]
81	5.889	8.28[10]	5.892	8.26[10]	5.890	8.28[10]	1.12[11]
82	5.556	9.83[10]	5.558	9.80[10]	5.556	9.83[10]	1.33[11]
83	5.244	1.17[11]	5.247	1.16[11]	5.245	1.16[11]	1.56[11]
84	4.952	1.38[11]	4.955	1.37[11]	4.953	1.38[11]	1.84[11]
85	4.679	1.63[11]	4.681	1.62[11]	4.679	1.63[11]	2.16[11]
86	4.423	1.92[11]	4.425	1.92[11]	4.423	1.92[11]	2.54[11]
87	4.182	2.27[11]	4.184	2.26[11]	4.182	2.26[11]	2.97[11]
88	3.956	2.67[11]	3.958	2.66[11]	3.956	2.67[11]	3.48[11]
89	3.744	3.13[11]	3.746	3.12[11]	3.744	3.13[11]	4.07[11]
90	3.545	3.68[11]	3.546	3.67[11]	3.544	3.68[11]	4.76[11]
91	3.357	4.31[11]	3.358	4.30[11]	3.356	4.31[11]	5.56[11]
92	3.180	5.05[11]	3.182	5.04[11]	3.180	5.05[11]	6.48[11]
93	3.014	5.91[11]	3.015	5.89[11]	3.013	5.91[11]	7.56[11]
94	2.857	6.91[11]	2.858	6.88[11]	2.856	6.90[11]	8.80[11]
95	2.709	8.06[11]	2.710	8.04[11]	2.708	8.06[11]	1.02[12]
96	2.569	9.40[11]	2.570	9.37[11]	2.568	9.40[11]	1.19[12]
97	2.437	1.10[12]	2.439	1.09[12]	2.436	1.10[12]	1.39[12]
98	2.313	1.28[12]	2.314	1.27[12]	2.312	1.28[12]	1.61[12]
99	2.195	1.48[12]	2.196	1.48[12]	2.194	1.48[12]	1.87[12]
100	2.084	1.72[12]	2.085	1.72[12]	2.082	1.72[12]	2.17[12]

<sup>a</sup>The total radiative decay rate of the  $(2s^2 2p_{1/2}^5 3s_{1/2})_{J=0}$  level is given in the last column.

for these two  $E1$  transitions is shown in Fig. 5 and compared to the rate for  $M1$  decay to the  $(2s^2 2p_{3/2}^5 3s_{1/2})_{J=1}$  level. We note that in the case of  $M1$  decay the core also must change angular momentum.

Looking at Fig. 5 we see a sharp discontinuity in the  $E1$  and  $M2$  decay rates of the  $(2s^2 2p_{1/2}^5 3s_{1/2})_{J=0}$  level. This is the result of an avoided crossing with the  $(2s^2 2p_{3/2}^5 3d_{3/2})_{J=0}$  level. These two levels mix strongly between  $Z = 50$  and  $Z = 51$ , and that mixing manifests itself in the decay rates.

The radiative lifetime of the  $(2s^2 2p_{1/2}^5 3s_{1/2})_{J=0}$  level is shown in Fig. 6. The level lifetime is given by the inverse of the sum of all radiative decay rates. It is decreasing swiftly with increasing atomic number and exhibits a dip around  $Z = 50$ , i.e., near the aforementioned avoided crossing of the  $(2s^2 2p_{1/2}^5 3s_{1/2})_{J=0}$  and  $(2s^2 2p_{3/2}^5 3d_{3/2})_{J=0}$  levels.

In Table I we present an overview of the wavelength of the  $(2s^2 2p_{1/2}^5 3s_{1/2})_{J=0} \rightarrow (2s^2 2p_{3/2}^5 3s_{1/2})_{J=1}$  transition, the associated  $M1$  decay rate, and the total radiative rate of the  $(2s^2 2p_{1/2}^5 3s_{1/2})_{J=0}$  calculated with FAC for neonlike ions with  $Z = 13$ –100. The table also lists the wavelength and transition

rate evaluated in first-order (RMBPT-I) and second-order RMBPT (RMBPT-II). For  $Z \geq 22$ , the differences between the RMBPT-II and RMBPT-I values are less than 3.5% for wavelengths and less than 11% for transition rates and give a measure of the correlation contribution. These differences diminish with increasing atomic number and nearly vanish at the highest  $Z$  listed. The differences between the FAC and RMBPT results for the radiative rates and wavelengths are also rather small and tend to lie between the two RMBPT calculations at the highest atomic numbers ( $Z \geq 68$ ). As the atomic number drops below  $Z = 22$ , the radiative rates calculated in first- and second-order RMBPT start to differ substantially. For  $Z = 14$  (silicon), the RMBPT-II radiative rate value is an order of magnitude smaller than the RMBPT-I value; for  $Z = 13$  (aluminum), the RMBPT-II value is four orders of magnitude smaller. The calculated wavelengths also drift apart. For  $Z = 13$  the difference is huge: the RMBPT-I value is 54,000 Å, while the RMBPT-II value is 987,000 Å. This behavior is likely due to cancellations, over which we have no control. We note that the RMBPT-I wavelength values are generally smaller

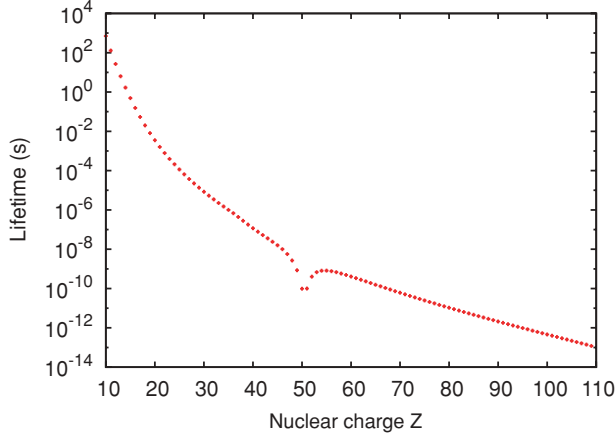


FIG. 6. (Color online) Radiative lifetime of the  $(2s^2 2p_{1/2}^5 3s_{1/2})_{J=0}$  level as a function of nuclear charge predicted by FAC calculations.

than the RMBPT-II values for all atomic numbers but  $Z = 20$ . The values from the FAC calculations (both wavelength and radiative rate) tend to agree more with those from RMBPT-I and, for the lowest atomic numbers, lie between the values calculated with first- and second-order RMBPT.

#### IV. DISCUSSION

The  $(2s^2 2p_{1/2}^5 3s_{1/2})_{J=0} \rightarrow (2s^2 2p_{3/2}^5 3s_{1/2})_{J=1}$  transition has been observed by the SUMER instrument aboard the SOHO spacecraft in the case of iron ( $Z = 26$ ) [11]. Its wavelength was measured to be  $1153.151 \pm 0.025$  Å, and we can compare this result to our calculated values. Not surprisingly, the second-order RMBPT calculation produces a wavelength value that is very close to the measured value. The other two calculations have produced wavelengths that are either too long or too short.

The wavelength values calculated in second-order RMBPT for the lowest atomic numbers differ substantially from the other two calculations, as mentioned above. We are not aware of any measurements to affirm this behavior of the RMBPT-II calculations. However, the database of the NIST [40] gives energy values for the  $(2s^2 2p_{1/2}^5 3s_{1/2})_{J=0}$  and  $(2s^2 2p_{3/2}^5 3s_{1/2})_{J=1}$  levels, from which we derive 63,044 Å, 40,312 Å, 26,510 Å, and 17,863 Å for the  $(2s^2 2p_{1/2}^5 3s_{1/2})_{J=0} \rightarrow (2s^2 2p_{3/2}^5 3s_{1/2})_{J=1}$  transition wavelength in Al IV, Si V, P VI, and S VII, respectively. The first three values are in better agreement with the RMBPT-I and FAC values than with the RMBPT-II values. The NIST value for S VII, however, agrees best with our RMBPT-II result. Clearly, measurements are needed to discriminate among the calculations.

The range of radiative lifetimes of the  $(2s^2 2p_{1/2}^5 3s_{1/2})_{J=0}$  level varies over 13 orders of magnitude for the range of  $Z$  given in Table I. It is possible to measure radiative lifetime in the range of roughly  $1 \times 10^{-2}$  to  $1 \times 10^{-7}$  s<sup>-1</sup> with an electron beam ion trap [14,41,42], as was originally demonstrated by Wargelin *et al.* [43]. It may also be possible to observe long-lived lifetimes with the Kingdon trap method [44]. Measurements of shorter lifetimes up to roughly  $1 \times 10^{-12}$  s<sup>-1</sup> are possible with the beam-foil technique [45,46], and even

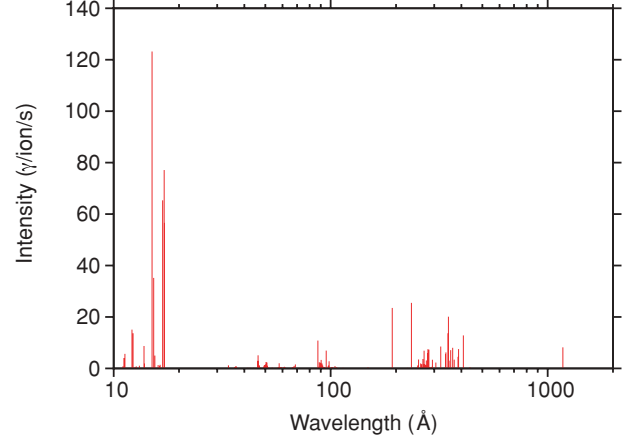


FIG. 7. (Color online) Predicted spectrum of Fe XVII from an electron beam ion trap with an assumed electron-beam energy of 1200 eV and an electron density of  $5 \times 10^{10}$  cm<sup>-3</sup>.

faster radiative decay rates have been measured with electron beam ion traps by studying the natural line shape of an emission line [47]. This means that almost the entire range of lifetimes in Table I is in principle open to measurement.

In Fig. 7 we show the spectrum of neonlike Fe<sup>16+</sup> calculated with FAC for typical conditions found in an electron beam ion trap, i.e., an electron density of  $5 \times 10^{10}$  cm<sup>-3</sup> and an electron-beam energy of 1200 eV. The strongest Fe XVII transition is due to the  $E1$  decay of the  $(2s^2 2p_{1/2}^5 3d_{3/2})_{J=1}$  level to ground at 15 Å. The intensity of the  $(2s^2 2p_{1/2}^5 3s_{1/2})_{J=0} \rightarrow (2s^2 2p_{3/2}^5 3s_{1/2})_{J=1}$  transition at 1153 Å is about 7% of that of the 15 Å line. This means this line should be observable in such experiments.

We note, however, that the  $(2s^2 2p_{1/2}^5 3s_{1/2})_{J=0} \rightarrow (2s^2 2p_{3/2}^5 3s_{1/2})_{J=1}$  transition is sensitive to the electron density. As the density increases, the intensity of the line diminishes. In Fig. 8 we quantify the density dependence of the relative intensity of the  $(2s^2 2p_{1/2}^5 3s_{1/2})_{J=0} \rightarrow (2s^2 2p_{3/2}^5 3s_{1/2})_{J=1}$  transition to that of the strong  $(2s^2 2p_{1/2}^5 3d_{3/2})_{J=1} \rightarrow (2s^2 2p^6)_{J=0}$  transition.

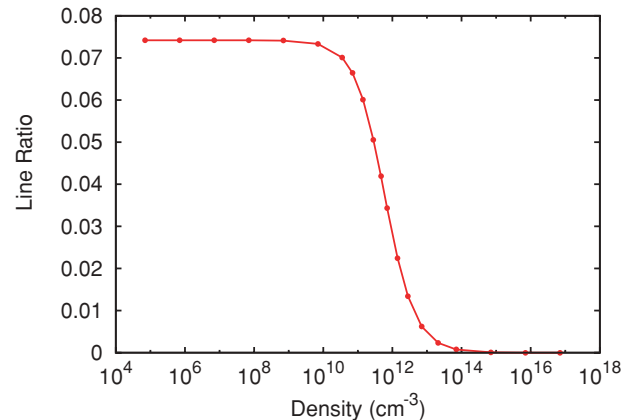


FIG. 8. (Color online) Density sensitivity of the intensity of the  $(2s^2 2p_{1/2}^5 3s_{1/2})_{J=0} \rightarrow (2s^2 2p_{3/2}^5 3s_{1/2})_{J=1}$  transition relative to that of the  $(2s^2 2p_{1/2}^5 3d_{3/2})_{J=1} \rightarrow (2s^2 2p^6)_{J=0}$  transition.

The density dependence precludes observation of the  $(2s^2 2p_{1/2}^5 3s_{1/2})_{J=0} \rightarrow (2s^2 2p_{3/2}^5 3s_{1/2})_{J=1}$  transition at electron densities that are too high. Thus, proper tuning of the electron beam is necessary to make such measurements. Measurements of the  $(2s^2 2p_{1/2}^5 3s_{1/2})_{J=0}$  lifetime thus provide not only a test of atomic theory but also valuable data for calibrating the density sensitivity of the associated  $M1$  transition. Moreover, measurements near  $Z = 50$  will be able to observe the effects of strong configuration interaction associated with adiabatic level crossings.

#### ACKNOWLEDGMENT

This work was performed under the auspices of the US Department of Energy by Lawrence Livermore National Laboratory under Contract No. DE-AC52-07NA27344 and supported by NASA's Astronomy and Physics Research and Analysis Program under Work Order No. NNG06WF08I. M. O. gratefully acknowledges support from the Deutscher Akademischer Austauschdienst (DAAD).

- 
- [1] P. Beiersdorfer, M. Bitter, S. von Goeler, S. Cohen, K. W. Hill, J. Timberlake, R. S. Walling, M. H. Chen, P. L. Hagelstein, and J. H. Scofield, *Phys. Rev. A* **34**, 1297 (1986).
- [2] P. Beiersdorfer *et al.*, *Phys. Rev. A* **37**, 4153 (1988).
- [3] P. Beiersdorfer, M. H. Chen, R. E. Marrs, and M. A. Levine, *Phys. Rev. A* **41**, 3453 (1990).
- [4] D. D. Dietrich, G. A. Chandler, R. J. Fortner, C. J. Hailey, and R. E. Stewart, *Phys. Rev. Lett.* **54**, 1008 (1985).
- [5] B. K. F. Young, A. L. Osterheld, R. S. Walling, W. H. Goldstein, T. W. Phillips, R. E. Stewart, G. Charatis, and G. E. Busch, *Phys. Rev. Lett.* **62**, 1266 (1989).
- [6] M. Klapisch, A. B. Shalom, J. L. Schwob, B. S. Fraenkel, C. Breton, C. de Michelis, M. Finkenthal, and M. Mattioli, *Phys. Lett. A* **69**, 34 (1978).
- [7] J. K. Lepson, P. Beiersdorfer, E. Behar, and S. M. Kahn, *Astrophys. J.* **625**, 1045 (2005).
- [8] J. Lepson, P. Beiersdorfer, J. Clementson, M. F. Gu, M. Bitter, L. Roquemore, R. Kaita, P. G. Cox, and A. S. Safronova, *J. Phys. B* **43**, 144018 (2010).
- [9] C. W. Mauche, D. A. Liedahl, and K. B. Fournier, *Astrophys. J.* **560**, 992 (2001).
- [10] C. W. Mauche, D. A. Liedahl, and K. B. Fournier, in *X-ray Diagnostics of Astrophysical Plasmas: Theory, Experiment, and Observation*, edited by R. K. Smith, AIP Conference Series, Vol. 774 (AIP, New York, 2005), p. 133.
- [11] U. Feldman, W. Curdt, E. Landi, and K. Wilhelm, *Astrophys. J.* **544**, 508 (2000).
- [12] P. Beiersdorfer, J. H. Scofield, and A. L. Osterheld, *Phys. Rev. Lett.* **90**, 235003 (2003).
- [13] P. Beiersdorfer, G. V. Brown, R. Goddard, and B. J. Wargelin, *Rev. Sci. Instrum.* **75**, 3720 (2004).
- [14] E. Träbert, *Can. J. Phys.* **86**, 73 (2008).
- [15] A. K. Bhatia, U. Feldman, and J. F. Seely, *At. Data Nucl. Data Tables* **32**, 435 (1985).
- [16] J. A. Cordogan and S. Lunell, *Phys. Scr.* **33**, 406 (1986).
- [17] E. Biémont and J. E. Hansen, *At. Data Nucl. Data Tables* **37**, 1 (1987).
- [18] H. Zhang, D. H. Sampson, R. E. H. Clark, and J. B. Mann, *At. Data Nucl. Data Tables* **37**, 17 (1987).
- [19] H. L. Zhang and D. H. Sampson, *At. Data Nucl. Data Tables* **43**, 1 (1989).
- [20] E. P. Ivanova and A. V. Gulov, *At. Data Nucl. Data Tables* **49**, 1 (1991).
- [21] A. Hibbert, M. Le Dourneuf, and M. Mohan, *At. Data Nucl. Data Tables* **53**, 23 (1993).
- [22] M. Cornille, J. Dubau, and S. Jacquemots, *At. Data Nucl. Data Tables* **58**, 1 (1994).
- [23] U. I. Safronova, C. Namba, I. Murakami, W. R. Johnson, and M. S. Safronova, *Phys. Rev. A* **64**, 012507 (2001).
- [24] J. R. Crepo López-Urrutia and P. Beiersdorfer, *Astrophys. J.* **721**, 576 (2010).
- [25] M. F. Gu, *Can. J. Phys.* **86**, 675 (2008).
- [26] U. I. Safronova, A. S. Safronova, and P. Beiersdorfer, *Phys. Rev. A* **77**, 032506 (2008).
- [27] J. H. Parkinson, *Astron. Astrophys.* **24**, 215 (1973).
- [28] A. C. Brinkman *et al.*, *Astrophys. J. Lett.* **530**, L111 (2000).
- [29] C. R. Canizares *et al.*, *Astrophys. J.* **539**, L41 (2000).
- [30] P. Beiersdorfer *et al.*, *Astrophys. J. Lett.* **576**, L169 (2002).
- [31] P. Beiersdorfer, M. Bitter, S. von Goeler, and K. W. Hill, *Astrophys. J.* **610**, 616 (2004).
- [32] M. F. Gu, e-print arXiv:0905.0519.
- [33] I. P. Grant, *J. Phys. B* **7**, 1458 (1974).
- [34] M.-F. Gu, *Astrophys. J.* **582**, 1241 (2003).
- [35] J. Clementson and P. Beiersdorfer, *Phys. Rev. A* **81**, 052509 (2010).
- [36] G. Y. Liang and G. Zhao, *Mon. Not. R. Astron. Soc.* **384**, 489 (2010).
- [37] W. R. Johnson, S. A. Blundell, and J. Sapirstein, *Phys. Rev. A* **37**, 2764 (1988).
- [38] G. V. Brown, P. Beiersdorfer, and K. Widmann, *Phys. Rev. A* **63**, 032719 (2001).
- [39] N. Nakamura, D. Kato, and S. Ohtani, *Phys. Rev. A* **61**, 052510 (2000).
- [40] [[http://physics.nist.gov/PhysRefData/ASD/levels\\_form.html](http://physics.nist.gov/PhysRefData/ASD/levels_form.html)].
- [41] J. R. Crespo López-Urrutia, P. Beiersdorfer, and K. Widmann, *Phys. Rev. A* **74**, 012507 (2006).
- [42] E. Träbert, P. Beiersdorfer, and G. V. Brown, *Phys. Rev. Lett.* **98**, 263001 (2007).
- [43] B. J. Wargelin, P. Beiersdorfer, and S. M. Kahn, *Phys. Rev. Lett.* **71**, 2196 (1993).
- [44] D. A. Church, *Phys. Rep.* **228**, 254 (1993).
- [45] I. Martinson and A. Gaupp, *Phys. Rep.* **15**, 113 (1974).
- [46] E. Träbert, in *Accelerator-Based Atomic Physics Techniques and Applications*, edited by S. M. Shafroth and J. C. Austin (AIP, Washington, DC, 1997), p. 567.
- [47] P. Beiersdorfer, A. L. Osterheld, V. Decaux, and K. Widmann, *Phys. Rev. Lett.* **77**, 5353 (1996).